J. Fluid Mech. (2004), *vol.* 520, *pp.* 327–342.
DOI: 10.1017/S0022112004001636 Printed in the United Kingdom

Sediment erosion by Görtler vortices: the scour-hole problem

By E. J. HOPFINGER[1], A. KURNIAWAN[2]†, W. H. GRAF[2] AND U. LEMMIN[2]

[1] LEGI, CNRS/INPG, 38041 Grenoble–Cedex 9, France

[2]Laboratoire de Recherches Hydrauliques, EPFL, Switzerland

(Received 13 October 2003 and in revised form 1 April 2004)

Experimental results on sediment erosion (scour) by a plane turbulent wall jet, issuing from a sluice gate, are presented which show clearly – it seems for the first time – that the turbulent wall layer is destabilized by the concave curvature of the water/sediment interface. The streamwise Görtler vortices which emerge create sediment streaks or longitudinal sediment ridges. The analysis of the results in terms of Görtler instability of the wall layer indicates that the strength of these curvature-excited streamwise vortices is such that the sediment transport is primarily due to turbulence created by these vortices. Their contribution to the wall shear stress is taken to be of the same form as the normal turbulent wall shear stress. For this reason, the model developed by Hogg *et al.* (*J. Fluid Mech.* Vol. 338, 1997, p. 317) remains valid; only the numerical coefficients are affected. The logarithmic dependency of the time evolution of the scour-hole depth predicted by this model is shown to be in good agreement with experiments. New scaling laws for the quasi-steady state depth and the associated time, inspired by the Hogg *et al.* (1997) model are proposed. Furthermore, it is emphasized that at least two scouring regimes must be distinguished: a short-time regime after which a quasi-steady state is reached, followed by a long-time regime, leading to an asymptotic state of virtually no sediment transport.

1. Introduction

Local scour downstream of hydraulic structures by a jet issuing from a sluice gate has received considerable attention because scour can endanger the foundations of the structure (see Graf & Altinakar 1998). The first systematic study of this problem dates back to Eggenberger & Mueller (1944) who proposed a correlation for the asymptotic scour-hole depth in terms of the hydraulic parameters. A number of other studies followed. Rajaratnam (1981) investigated the scour hole shape in some detail and showed that the depth of the scour scales with the jet nozzle size and the densimetric particle Froude number, $Fr_d = U_0/\sqrt{g(\Delta\rho/\rho)d_{50}}$ (symbols are defined later). Most of the experiments considered submerged plane water jets impinging on, or flowing parallel to, a mobile sediment bed. Round jets as well as air jets (Rajaratnam & Berry 1977) and pulsating jets (Kobus, Leister & Westrich 1979) and different entrance length of the jets or different water depths (Chatterjee, Ghosh & Chatterjee 1994)

† Present address: Civil Engineering Department, Faculty of Engineering, Gadjah Mada University, Yogykarta, Indonesia.

were also investigated. A partial summary of the existing experimental data is given by Karim & Ali (2000).

A much debated question is the time it takes for a scour hole to form. It is observed that initially the deepening rate is large (short-time regime) and a quasi-steady state is reached in a few hundred seconds (depending on the jet size). Then, deepening continues for days at a very slow rate (Kurniawan, Altinakar & Graf 2001) until the asymptotic depth is reached. During the first short-time regime of scouring, the scour hole reaches about half its asymptotic depth.

A remarkable theoretical model of the progressive erosion of a loose sediment bed by a two-dimensional wall jet has been developed by Hogg, Huppert & Dade (1997, hereinafter referred to as HHD). These authors used a mass conservation equation which includes the variation of the erosive force with flow parameters and the effect of the changing bed characteristics on the effective sediment transport in the scour hole. Its calculated shape was shown to be in reasonably good agreement with the experiments. The time variations of the scour-hole depth are also given by this model, but no direct comparison with the experiments was made.

None of the publications mention the possibility of a curvature-dependent instability of the boundary layer. The scour hole which is formed by the turbulent wall jet has a concave shape, and Görtler instability in the wall region of the jet is likely to occur. Such an instability can drastically change the turbulence structure and substantially alter the sediment transport rate. It can even be conjectured that this instability and the ensuing strong streamwise vortices are at the origin of the erosion in the long-time regime because these vortices, besides giving rise to strong sediment movement, also cause suspended load formation which is carried out of the hole.

In this paper, it is shown (§ 3) that the pattern of bed-load transport is indicative of the existence of streamwise vortices. According to the Görtler instability criteria of a turbulent boundary layer on a concave wall given by Tani (1962) and the turbulent wall jet studied by Kobayashi & Fujisawa (1983), these vortices originate from centrifugal instability. The contribution of these vortices to the wall shear stress or more precisely to the effective shear stress (see § 3.3) is evaluated. The time evolution of the scour-hole depth is then analysed (§ 4) in the context of the HHD model also giving scaling laws for the quasi-steady state (called steady state by HHD). Further discussion and conclusions are presented in § 5.

2. Experimental installation and conditions

The hydraulic flume used is shown schematically in figure 1(*a*). It consists of a 14 m long horizontal channel, 80 cm deep and 50 cm wide. At the upstream and downstream ends of this channel the bottom was raised by inserting rigid panels about 5 m in length in order to create a 35 cm deep and 3.80 m long cavity in the middle of channel. The latter was filled with uniformly graded sand of mean grain diameter $d_{50} = 2$ mm. The upper surface of this mobile sand bed was initially flush with the upstream panel. A sluice gate was installed either at the beginning of the sand bed or at a short distance, L_f, upstream. In most of the experiments reported here, the sluice gate was located 10 cm upstream of the start of the sediment bed. The gate opening was $b_0 = 2.5$ cm to 8 cm, but most of the experiments were conducted with $b_0 = 5$ cm (see table 1). The downstream water depth was kept constant during the experiments at $h_2 \approx 22$ cm and the upstream water depth, h_1, was adjusted so as to give the desired initial (jet) velocity, $U_0 = \sqrt{2g\Delta h}$, where $\Delta h = h_1 - h_2$. The water depths were monitored with ultrasonic probes connected to a PC. The velocity U_0 could be varied up to 1.30 m s^{-1}.

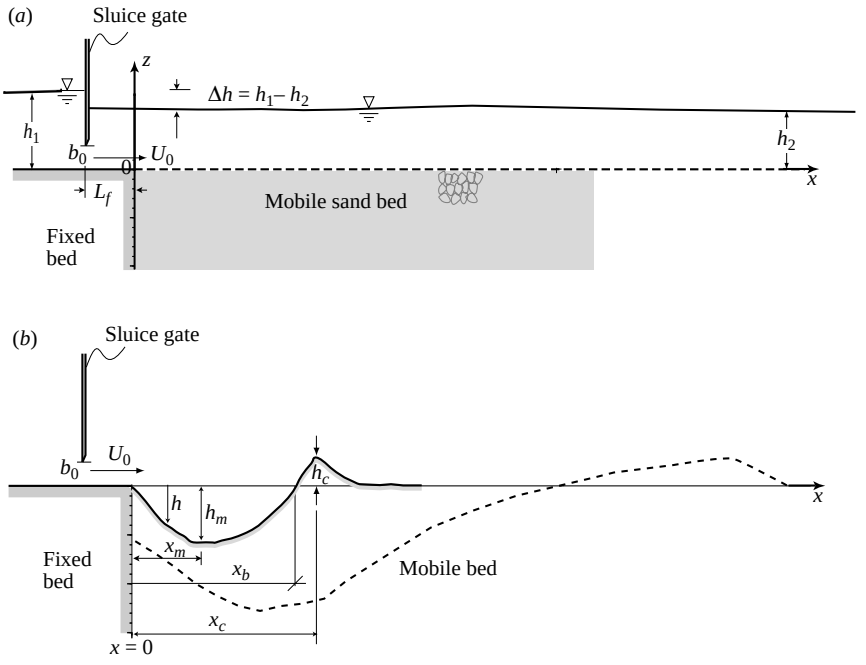

FIGURE 1. (*a*) Schematic representation of the experimental installation. (*b*) Definition of the scour hole dimensions. —, scour-hole form $(h_m(t_s) = h_s)$; - - -, asymptotic state of depth, $h_a = \lim(h_m) \overset{t}{\longrightarrow} \infty$ and length $L_a = \lim(x_b) \overset{t}{\longrightarrow} \infty$.

For the grain size of the present experiments, the critical Shields parameter (see Graf 1971) for incipient motion over an almost flat bed is $\tau^*_{crit} = \tau_b/(\rho_s - \rho)\, g d_{50} = 0.035$, where τ_b is the bed shear stress. The velocity for incipient motion was measured to be $U_{0\,crit} = 41\ \mathrm{cm\,s^{-1}}$, which fits well with the Hjulstrom diagram (see Graf 1971). This gives a friction coefficient of $c_f = \tau_b/(\rho U_0^2/2) = 0.014$, a value representative of fully rough conditions (see Schlichting 1968; Grass 1971).

Commencing the experiments, the mobile bed was covered with a thin plate about 1 m long and the water levels were adjusted to the desired values. At time $t = 0$, this plate was suddenly withdrawn (pulled upstream along the upstream rigid boundary). This had no effect on the start of the erosion; the critical velocity, for instance, was the same with or without the plate. After withdrawal of the plate, scouring progressed rapidly and the scour hole reached in time $t = t_s$, a quasi-steady-state depth, $h_s = h_m(t_s)$ and, equivalently, a length, $L_s = x_b(t_s)$. In the experiments, t_s is of the order of a hundred seconds. The characteristic dimensions of the scour hole are shown in figure 1(*b*).

The scour-hole shape as a function of time was determined from side-view video images taken with a digital video camera. The sediment movement in the scour hole and its variation across the width of the channel was observed with a second video camera positioned near the gate and looking downstream (at an angle to the flow direction). Dye injection indicated that the jet remained attached to the sediment surface. When approaching the quasi-steady-state scour hole conditions, a very small (thin) separation bubble exists on the downstream-facing sediment slope and near to the beginning of the mobile bed, but this does not prevent centrifugal instability occurring.

Test	b_0 (m) $\times 10^{-2}$	L_f (m) $\times 10^{-2}$	Δh (m) $\times 10^{-2}$	U_0 [m s^{-1}]	n, number of streaks observed	$\lambda = B/n$ (m)	$\alpha = 2\pi/\lambda$ (m^{-1})	θ (m) $\times 10^{-3}$	$\alpha\theta$	R, radius (m)	G_T	t_s, quasi-steady state (s)
B	5.00	0	3.65	0.846	NA	NA	NA	NA	NA	0.195	NA	NA
C	5.00	10	3.62	0.843	NA	NA	NA	NA	NA	0.207	NA	NA
2305	5.00	10	7.50	1.213	~ 7	0.071	87.92	2.41	0.212	0.235	3.136	170
2805	5.00	10	1.96	0.620	~ 6	0.083	75.36	1.46	0.110	0.165	2.911	240
2905	5.00	10	3.90	0.874	~ 7	0.071	87.92	1.89	0.166	0.209	2.944	240
3005*a*	8.00	10	3.94	0.879	~ 5	0.1	62.800	2.41	0.151	0.254	3.020	600
3005*b*	2.50	10	5.44	1.032	~ 8	0.063	100.48	1.34	0.135	0.118	3.309	180

TABLE 1. Summary of the experimental conditions and the calculated Görtler numbers. The momentum thickness, θ, is evaluated at $x = 1.7x_m$ (see figure 3*a*) using (2), and $c_f = 0.014$. The wavenumber, α, is determined from the maximum number of observed sediment streaks. NA stands for not available.

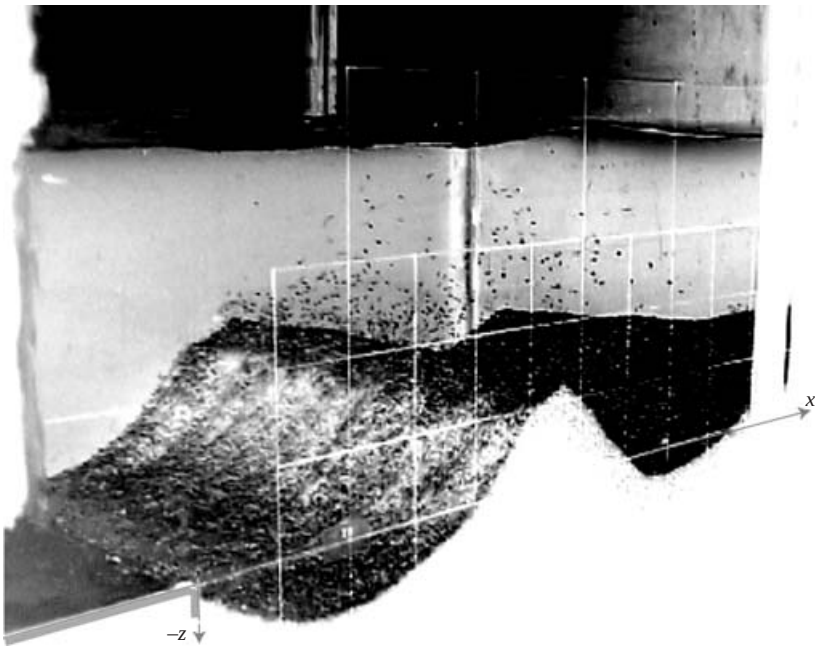

FIGURE 2. Streamwise oblique view of the sediment surface showing 8 longitudinal sediment streaks or ridges on the upstream-facing scour-hole slope.

3. Observation of erosion by curvature-driven streamwise vortices

3.1. *Qualitative observations*

A typical and good-quality instantaneous image of loose sediment streaks, indicative of sediment lift-up by the longitudinal vortices, is shown in figure 2. These streaks appear and disappear in a random fashion and their number varies somewhat in time. In this image, about 8 sediment streaks or ridges can be identified. The origin of these streaks and consequently the vortices can only be attributed to curvature-driven instability (known as Görtler vortices). Corner vortices would be much weaker, more permanent and would be present from the beginning of the sediment layer. When a vertical barrier was introduced parallel to the flow at different spanwise locations, the streak pattern was not altered.

From such images, the scour-hole depth as a function of time, $h_m(t)$, the radius of curvature, R, and the spacing of the sediment streaks, λ, were determined. The number of streaks, n, (for each instance of time) allowed the calculation of the wavelength, λ, and the wavenumber, α, or:

$$\lambda = B/n, \quad \alpha = 2\pi/\lambda, \tag{1}$$

where $B = 0.5$ m is the width of the flume.

A side view of the erosion process with the corresponding streamwise oblique view of the scour hole in experiment (Test 2905, see table 1) is shown in figures 3(*a*) and 3(*b*). While in the picture shown (taken at $t = 24.6$ s from the start) 6 streaks are evident, pictures taking at other instants of time, indicated that the number of streaks varied between 5 and 9 and the counting of the streaks, as given in table 1, was somewhat subjective. The number given in this table for each experiment is a mean value of several pictures.

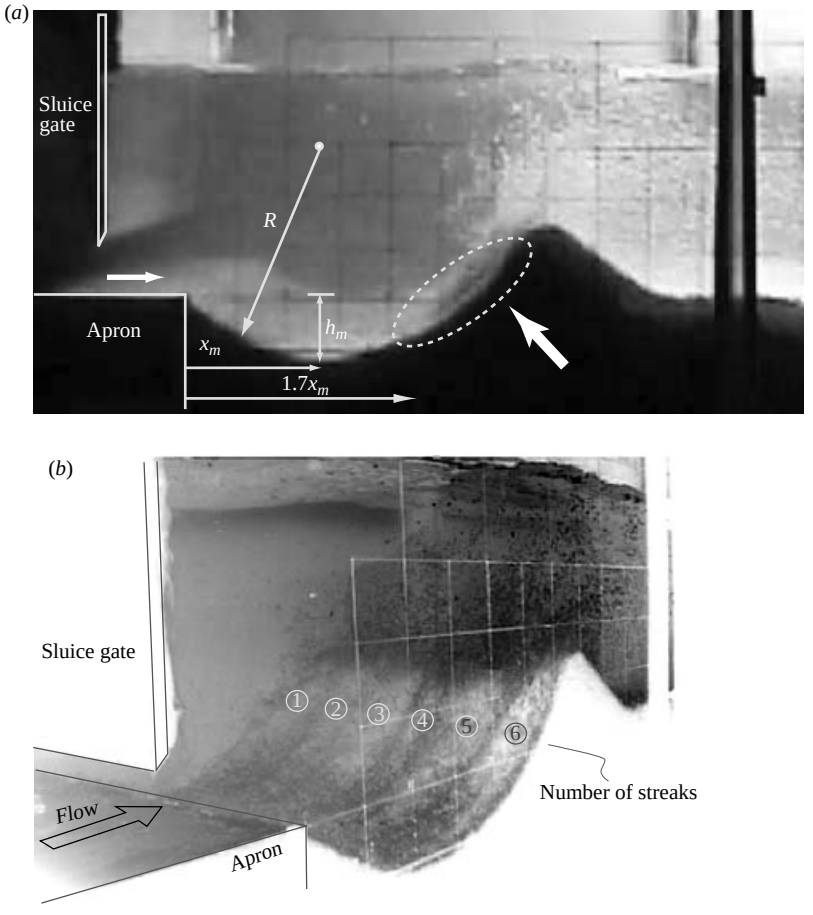

FIGURE 3. (*a*) Side view of sediment/water interface for Test 2905 ($U_0 = 0.874\,\mathrm{m\,s^{-1}}$ at time $t = 24.6$ s). The sediment cloud formed by the Görtler vortices is indicated by the arrow; (*b*) corresponding streamwise view direction showing the longitudinal sediment streaks formed by Görtler vortices.

3.2. *Analysis of the observations*

In order to demonstrate that the longitudinal vortices are of the Görtler type, it is necessary to calculate a Görtler number. For a laminar boundary layer this number is usually defined by $G = Re_\theta(\theta/R)^{1/2}$, where θ is a viscous length scale, often taken as equal to $(\nu x/U)^{1/2}$ or equal to the momentum thickness, R is the radius of curvature and $Re_\theta = U\theta/\nu$ the Reynolds number based on this length scale and the free-stream velocity (Schlichting 1968). Görtler (1941) considered the flow to be parallel, which allowed a normal mode analysis. Hall (1983) pointed out that, strictly speaking, a normal mode solution is not possible and that it is necessary to treat the full non-parallel problem which depends on initial conditions. Since then, a number of studies have dealt with the non-parallel instability problem (see for instance Hall 1990; Luchini & Bottaro 1998; Bottaro & Luchini 1999). Nevertheless, locally parallel theories, reviewed by Floryan (1991) and Saric (1994), continue to be used because

these are more convenient to deal with. Saric (1994) points out that the difference in growth rate of the perturbations obtained by a normal mode analysis and marching solutions is modest except near the leading edge. This conclusion is in agreement with the theoretical results of Bottaro & Luchini (1999).

The flow in the scour hole we are dealing with here is turbulent and of the wall-jet type. Görtler instability of a laminar wall jet has been considered theoretically by Floryan (1989), and experimentally by Matsson (1995). Matsson compared his results with the solutions of Floryan (1989). These experiments show that, sufficiently far downstream, the vortex amplitude tends to be practically independent of the initial conditions. The instability conditions of a turbulent wall jet on a concave surface were determined theoretically by Fujusawa & Shirai (1986) and investigated experimentally by Kobayashi & Fujisawa (1983). In these studies, the wall jet is fully developed before moving onto the concave boundary and the stability criterion introduced is $b/R \approx 0.2$, where b is the half-thickness of the wall jet. In the present geometry, the wall jet is not fully developed (the potential core region extends well into the scour-hole region) so that the half-thickness, b, is not well defined. We, therefore, prefer to work with wall conditions using the momentum thickness, θ as the characteristic scale, and, hence, boundary-layer instability. The instability criterion $b/R > 0.2$ is, however, well satisfied in the present experiments. The momentum thickness can be determined from the relation, $c_f \cong 2\mathrm{d}\theta/\mathrm{d}x$ (Schlichting 1968) giving

$$\theta \approx \tfrac{1}{2} c_f x + \theta_0, \tag{2}$$

where θ_0 is the momentum thickness at the gate outlet, $x = 0$. Its value is an order of magnitude smaller than the other term and is, therefore, neglected. In his analysis of experiments with a turbulent boundary layer on a concave wall, Tani (1962) defined the Görtler number in terms of eddy viscosity, ν_T and θ, and argued that by replacing the kinematic viscosity by the eddy viscosity, the laminar-boundary-layer Görtler-instability diagram can be used to determine the instability characteristics of a turbulent boundary layer. The eddy viscosity is $\nu_T = 0.018\, U_m\, \delta^*$, independent of roughness (Clauser 1956); U_m is the maximum velocity of the wall jet. The relation between displacement and momentum thickness depends on roughness and for fully rough conditions $\delta^* \approx 1.8\theta$ (Antonia & Luxton 1971). Subsequently, the turbulent Görtler number is given by

$$G_T = \frac{U_m \theta}{\nu_T} \sqrt{\frac{\theta}{R}} \approx 31 \sqrt{\frac{\theta}{R}}. \tag{3}$$

Table 1 summarizes the experimental conditions and the values of the Görtler number. The wavenumbers, α, are the values determined from the sediment streaks. The Görtler numbers are well above the critical value, below which Görtler vortices do not exist. This is clearly seen in figure 4 where the experimental values are presented in the Görtler number–wavenumber diagram of Tani (1962). The curves of the constant non-dimensional amplification rate correspond to $\sigma\theta Re_\theta \approx 31\sigma\theta$. Note that this instability diagram is very similar to that obtained by local normal mode analysis of a laminar boundary layer (see figure 3 of Saric 1994) but with the turbulent Görtler number replacing the one for a laminar boundary layer. As mentioned before, a normal mode analysis is, strictly speaking, not correct. It gives, nevertheless, a good indication of the spatial amplification rate and the wavelength (Saric 1994; Bottaro & Lichini 1999). It is seen from figure 4 that the experimentally determined (determined from the number of observed sediment ridges) non-dimensional wavenumber, $\alpha\theta$, is greater by about a factor of two than the expected most-amplified theoretical value. In our experiment,

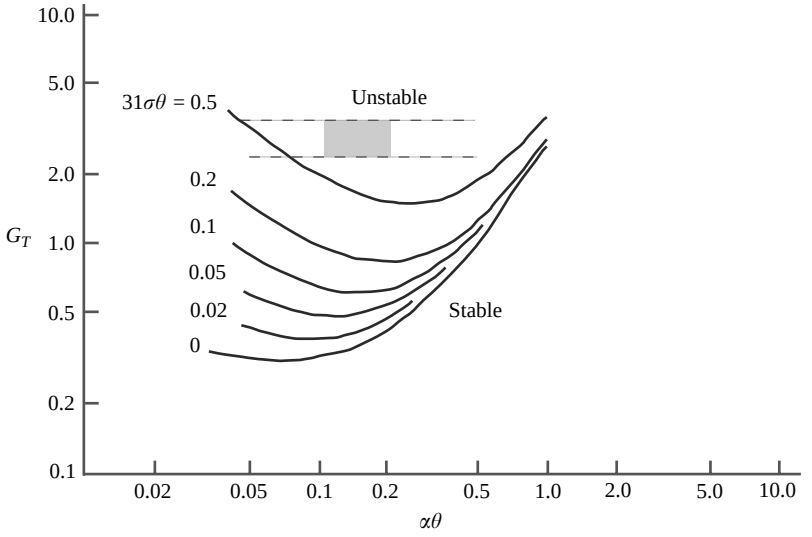

FIGURE 4. Non-dimensional wavenumber, $\alpha\theta$, versus the Görtler parameter (Tani 1962), $G_T = 31(\theta/R)^{1/2}$. The present data are in the shaded region. The curves of constant amplification rate, σ, are from Tani (1962).

the Görtler vortices are not steady; these come and go in a random manner. The images shown (figures 2 and 3) are instantaneous images. Because of this randomness, we think that only the larger stronger vortices, which can carry a sediment load, survive long enough to carry sediment up the bed slope. There is, therefore, a tendency for the sediment streak spacing to give an upper limit of the actual wavelength. Nevertheless, the observed wavelength corresponds to a non-dimensional wavenumber of about 0.2, a value often observed in experiments with equivalent Görtler numbers of a laminar boundary layer (see Saric 1994). In general, Görtler instability is very sensitive to outside perturbations so that the experimentally observed wavelengths vary easily by a factor of two or more. For a turbulent boundary layer the value is also about $\alpha\theta = 0.2$ (see Tani 1962). Floryan (1991) mentions a value of $\lambda/\delta \approx 2$ and Meroney & Bradshaw (1974) give $\lambda/\delta \approx 1.1$, where δ is the turbulent boundary-layer thickness. This gives $\alpha\theta \approx 0.15$ to 0.3 because $\delta \approx 10\theta$. The experiments with a turbulent wall jet by Kobayashi & Fujisawa (1983) correspond to turbulent Görtler numbers close to the present experiments. Their image of the flow taken perpendicular to the mean velocity (their figure 15) indicates eruptions, which correspond to our streaks, spaced by $\lambda \approx 25\theta$; this is close to our observations. The analysis of the observations in terms of Görtler instability, producing vortices, supports the claim that the observed sediment streaks are indeed a signature of Görtler vortices.

3.3. *Contribution of the Görtler vortices to sediment transport*

It will be assumed that the shear stresses due to the boundary-layer turbulence and due to the Görtler vortices are additive (in the same sense as turbulent kinetic energies are additive), giving a total effective shear stress, $\tau_b = \tau_t + \tau_G$. The turbulent shear stress is $\tau_t = \rho u_*^2 = \rho(c_f/2)U_m^2$ (see Schlichting 1968) where U_m is the velocity maximum of the wall jet, equal to U_0 in the potential core region. The shear stress due to Görtler vortices will be expressed in a similar way, $\tau_G = K\rho u_G^2 = \rho(c_{fG}/2)U_m^2$.

The total shear stress can thus be written as

$$\tau_b = \tfrac{1}{2} c_f \left(1 + \frac{c_{fG}}{c_f}\right) \rho U_m^2. \tag{4}$$

The velocity of the Görtler vortices may be evaluated from $u_G = u_1 \exp(\sigma x)$. The spatial amplification rate, σ, is obtained from figure. 4 which shows that, for the present experiments, 31 $\sigma\theta \approx 1$, giving $\sigma \approx 0.16\,\mathrm{cm}^{-1}$. This gives $\exp(\sigma x) \approx 25$ at the location $x \approx 1.7 x_m$, in the present experiments on average about 20 cm, and $u_G \approx 0.25 U_m$ when the initial perturbation is taken as $u_1 \approx 10^{-2} U_m$. This is less than the r.m.s. turbulent velocity because only turbulent velocities of scales comparable with the Görtler vortex spacing λ are likely to be amplified into Görtler vortices. With these values, we obtain $c_{fG} \approx 0.06$ when $K = 0.5$, implying that u_G is taken to be equivalent to a turbulent velocity. This assumption is justified because, for large Görtler numbers, the vortices are not steady and behave like turbulence. Kobayashi & Fujisawa (1983) included them, therefore, in the their turbulence measurements. A value of $K \approx 0.5$ is considered to be representative of the ratio of turbulent shear stress to turbulent kinetic energy which is usually 0.3, hence $K = (\tau_G/\rho)/u_G^2 \approx 0.5$. The velocity at which incipient sand grain motion occurs is close to $U_{0\,crit} = 0.41\,\mathrm{m\,s}^{-1}$ and the friction coefficient is $c_f = 0.014$. Substituting the values for c_f and c_{fG} into (4) gives $\tau_b \approx 0.007(1+4)\rho U_m^2$. This value of the shear stress is close to the value measured, for similar values of the Görtler numbers, in the wall region of a turbulent wall jet by Kobayashi & Fujisawa (1983). According to these values, Görtler vortices represent an important mobilizing force in the scouring process. Note also that τ_b is here an effective shear stress, active in sediment transport, and is not the shear stress at the wall, which is likely to increase only by about 50% owing to the increase of the mean shear by the Görtler vortices (Floryan 1991). In the downwash regions, the increase in wall shear stress is likely to be larger. Sediment is easily moved nearly horizontally at the wall by the increased wall shear stress in the downwash regions and lifted up by the vortices in the upwash regions to form ridges, thus exposing the sediment to high mean velocities. Vortices are, therefore, very efficient in transporting sediment. This is what we refer to as effective wall shear stress.

4. The HHD model

The HHD model does not explicitly take into account the sediment transport by Görtler vortices. However, if as proposed above, the transport by Görtler vortices is of the same form as the standard turbulence transport, the HHD model remains valid; only the effective shear stress is increased by a constant factor. This is a simplification because the strength of the Görtler vortices increases somewhat with depth as the radius of curvature decreases. For simplicity, we did not include this refinement in § 3.3. The HHD model shows a logarithmic dependency of the scour-hole depth on time. This logarithmic dependency has been pointed out by Rajaratnam (1981), however, no comparison with experiments of the depth–time evolution in terms of the suggested scaling laws has been attempted previously.

HHD obtained the temporal evolution of the scour-hole depth from the integration of the sediment conservation (Exner) equation (Graf 1971)

$$(1-p)\frac{\partial h}{\partial t} + \frac{\partial q_b}{\partial x} = 0, \tag{5}$$

where p is the porosity of the sediments of the bed, and q_b is the volumetric bed load flux per unit width which was assumed to be given by the Meyer–Peter and Muller-relation (see Graf 1971)

$$q_b = 8\left(\Delta\rho\, g d_{50}^3/\rho\right)^{1/2}(\tau^* - \tau_c^*)^{3/2}. \tag{6}$$

The critical shear stress parameter τ_c^* with respect to τ_{crit}^* depends on the bed slope angle, β, and the angle of repose, φ, in the form

$$\tau_c^* = \tau_{crit}^* \frac{\sin(\varphi + \beta)}{\sin\varphi}. \tag{7}$$

The expression derived by HHD (their equation (4.1)) for the bed shear stress, $\tau_b = \tau^* \Delta\rho\, g d_{50}$ in (6) is

$$\tau_b = C_6 \rho U_0^2 (b_0/d_{50})^{2\gamma} (x/b_0)^{-1+\gamma} G(h, x), \tag{8}$$

where $G(h, x)$ is a shape function for describing how the bed shear stress varies when the boundary is no longer horizontal. It is assumed in the model that $G(h, x) = 1$ when $h = 0$ and Gaussian, $G(h, x) = \exp(-(h/C_7\,\delta)^2)$ when $h < 0$. Here, $\delta(x)$ is the boundary-layer (wall region) thickness of the wall jet and C_7 is another constant. Furthermore, HHD give for the exponent $\gamma = -0.1$. This accounts for the momentum loss of the wall jet by bottom friction. The dependency of τ_b on (x/b_0) in (8) is for an established wall jet where the velocity maximum decays as $(b_0/x)^{0.47}$ (see Rajaratnam 1976). In the present case, the wall jet is not established and over part of the erosion zone, up to about 20 cm, the velocity maximum remains, therefore, close to U_0 .

In order to express (5) in non-dimensional form, HHD introduced, respectively, the following length, time and sediment flux scales:

$$H = b_0 \Theta^{1/(1-\gamma)}, \tag{9}$$

$$T = \frac{(1-p)\, b_0^2\, \Theta^{2/(1-\gamma)}}{8\left(\tau_{crit}^{*3}\, \Delta\, \rho g d_{50}^3/\rho \tan^3\varphi\right)^{1/2}}, \tag{10}$$

and

$$Q = 8\left(\tau_{crit}^{*3}\, \Delta\, \rho g d_{50}^3/\rho \tan^3\varphi\right)^{1/2}, \tag{11}$$

where

$$\Theta = C_6\, \rho U_0^2 (b_0/d_{50})^{2\gamma}\, \frac{\tan\varphi}{\Delta\, \rho g d \tau_{crit}^*} \tag{12}$$

is an erosion parameter. The length scale H emerges as a natural choice from the critical shear stress condition (equation (4.3) in HHD). The time and flux scales are more arbitrary, but the relations between the scales are imposed by the transport equation, (5). The adjustable constant C_6 in (8) and (12) should be of the order of $c_f/2$ ($c_f = 0.014$).

Here, we are not interested in solving the sediment conservation equation or in re-examining the scour-hole shape, but rather in verifying the scaling laws (9) to (11) proposed by HHD. In figure 5, the maximum scour-hole depth, $h_m(t)$ is plotted as a function of the logarithm of time. This figure indicates that, for all tests, the time evolution is similar and, to a good approximation, logarithmic. In figure 6, the non-dimensionalized scour-hole depth, $h_m^* = h_m/H$, is plotted as a function of the logarithm of the non-dimensional time, $t^* = t/T$. We varied $10^{-3} \leqslant C_6 \leqslant 10^{-1}$ and the best collapse of the data is obtained for $C_6 \approx 10^{-2}$. This collapse of all data onto one curve is a remarkable result of the HHD model.

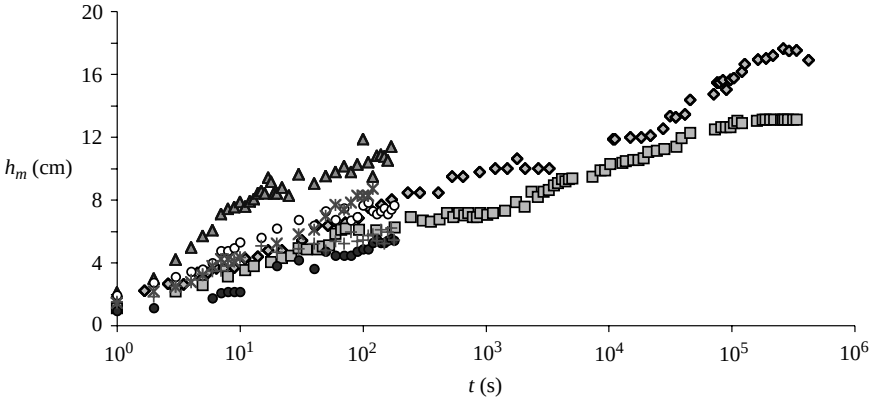

FIGURE 5. Maximum scour depth h_m versus the logarithm of time. ◇, $U_0 = 0.846\,\mathrm{m\,s^{-1}}$, $b_0 = 5\,\mathrm{cm}$; □, $U_0 = 0.843\,\mathrm{m\,s^{-1}}$, $b_0 = 5\,\mathrm{cm}$; ▲, $U_0 = 1.213\,\mathrm{m\,s^{-1}}$, $b_0 = 5\,\mathrm{cm}$; ●, $U_0 = 0.620\,\mathrm{m\,s^{-1}}$, $b_0 = 5\,\mathrm{cm}$; ○, $U_0 = 0.874\,\mathrm{m\,s^{-1}}$, $b_0 = 5\,\mathrm{cm}$; ×, $U_0 = 0.879\,\mathrm{m\,s^{-1}}$, $b_0 = 8\,\mathrm{cm}$; +, $U_0 = 1.032\,\mathrm{m\,s^{-1}}$, $b_0 = 2.5\,\mathrm{cm}$.

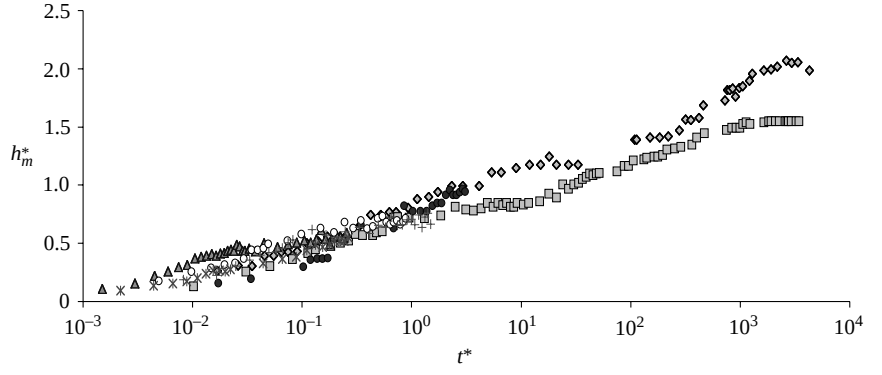

FIGURE 6. Non-dimensional maximum scour-hole depth, h_m^* versus the logarithm of adimensional time, $t^*(h_m^* = h_m/H,\ t^* = t/T)$. $C_6 = 0.01$, $p = 0.35$, $\tau_{crit}^* = 0.035$, $\gamma = -0.1$ and $\varphi = 33°$. For definition of symbols see figure 5.

It can be seen from figure 5 and more evidently from figure 8, that there are at least two regimes of scouring. The first reaches up to $t^* \approx 1$, during which the scour hole deepens rapidly and corresponds in the present experiments to about 100 s. During the second regime, the scour hole deepens intermittently at a very slow rate up to the asymptotic state. The data of Tests B and C show that after the first regime, the deepening rate is practically zero for a certain time (plateau in the curves) and then slowly increases again to reach another plateau and this behaviour continues up to the asymptotic state. The HHD model applies to the first active sediment transport regime, after which the scour-hole depth, h_s, is more than half the asymptotic depth, h_a, reached after hours or even days.

The sediment is eroded by the bed shear stress, strongly enhanced by the Görtler vortices and is carried up the upstream-facing slope at $x > x_m$. When the slope angle, β, is close to the angle of repose, φ, the sediment is still carried up the slope by the Görtler process, but is deposited before reaching the top at $x = x_c$. It first accumulates there and then moves downslope in the form of intermittent avalanches. This is referred to as the quasi-steady-state scour depth, called 'steady state' by HHD. We

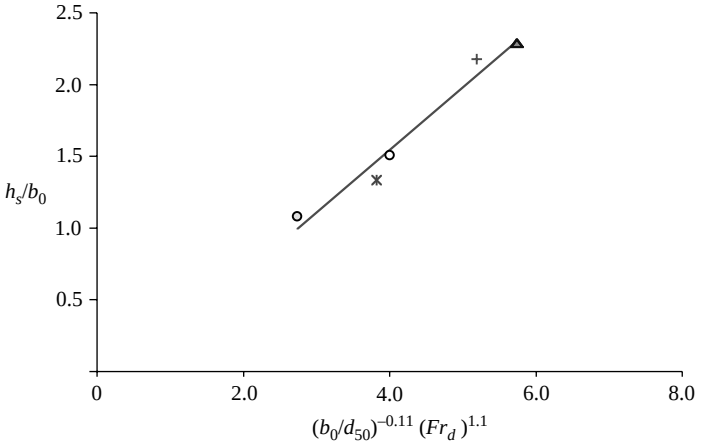

FIGURE 7. Maximum quasi-steady-state scour-hole depth normalized by b_0, h_s/b_0 versus $[(b_0/d_{50})^{-0.11}(Fr_d)^{1.1}]$. ▲, $U_0 = 1.213\,\mathrm{m\,s^{-1}}$, $b_0 = 5\,\mathrm{cm}$; ○, $U_0 = 0.620\,\mathrm{m\,s^{-1}}$, $b_0 = 5\,\mathrm{cm}$; ○, $U_0 = 0.874\,\mathrm{m\,s^{-1}}$, $b_0 = 5\,\mathrm{cm}$; ∗, $U_0 = 0.879\,\mathrm{m\,s^{-1}}$, $b_0 = 8\,\mathrm{cm}$; +, $U_0 = 1.032\,\mathrm{m\,s^{-1}}$, $b_0 = 2.5\,\mathrm{cm}$.

call it 'quasi-steady' instead of steady, because scouring continues at a very low rate by weak suspended load transport and by an intermittent rearrangement of the upstream facing bed slope. The sand wave crest at $x = x_c$ is slowly modified by sediment deposit before the crest and intermittent downslope motions of relatively large portions of sediment. This can result in a decrease of the slope angle and a slight downstream displacement of a wave crest, decreasing intermittently the slope angle, thus allowing for a renewal of scouring.

Of practical interest are the asymptotic scour-hole depth, h_a, and scour length, L_a. ($h_a = \lim(h_m) \overset{t}{\longrightarrow} \infty$ and idem for L_a). Various correlations have been proposed for h_a (e.g. Eggenberger & Mueller 1944; Rajaratnam 1981; Ali & Lim 1986). The latter are of the form $h_a/b_0 \propto Fr_d$ or $h_a/b_0 \propto (U_0/v_{ss})^{1/2} Fr_d^{3/4}$, where v_{ss} is the particle settling velocity and $Fr_d = U_0/\sqrt{g(\Delta\rho/\rho)\,d_{50}}$. Experiments show (see figure 5 and Kurniawan, Altinakar & Graf 2004) that $h_a = c_1 h_s$ and $L_a = c_2 L_s$, where $h_s = h_m(t_s)$, (the same for L_s) and t_s is the time at which the quasi-steady state is reached. The constants are approximately $c_1 \approx 1.9$ and $c_2 \approx 1.7$. The dependency of h_a or h_s on U_0 in these correlations is of the form h_s or $h_a \propto U_0^{\ell}$ with $\ell \approx 1$. The characteristic length scale H of HHD, equation (9), has an exponent ℓ close to 2. It is possible to adapt the HHD scaling, (9), to h_s in the form:

$$H_s = b_0 f_1(\Theta), \tag{13a}$$

with $f_1(\Theta) = (\Theta^{1/(1-\gamma)})^a$ such that the characteristic length scale is

$$H_s = b_0\left(\Theta^{1/(1-\gamma)}\right)^a. \tag{13b}$$

The exponent a in (13b) is determined from the experimentally observed dependency of h_s on U_0 and b_0 for, otherwise, the same conditions. First, we determine the exponent ℓ in $h_s \propto U_0^{\ell}$, keeping the other variables constant. The best fit is obtained with $\ell = 1.1$, but $\ell = 1$ would also be acceptable. The range of U_0 is too narrow to decide definitely, but arguments given below support $\ell = 1.1$. When taking $\ell = 1.1$, the corresponding exponent a in (13a) is close to 0.6, giving

$$\left(\Theta^{1/(1-\gamma)}\right)^{0.6} = \left[C_6 \frac{\tan\varphi}{\tau^*_{crit}}\right]^{0.6/1.1} \left(\frac{b_0}{d_{50}}\right)^{-0.11} Fr_d^{1.1}. \tag{14}$$

In figure 7, h_s/b_0 is plotted as a function of $(b_0/d_{50})^{-0.11} Fr_d^{1.1}$. The best fit is

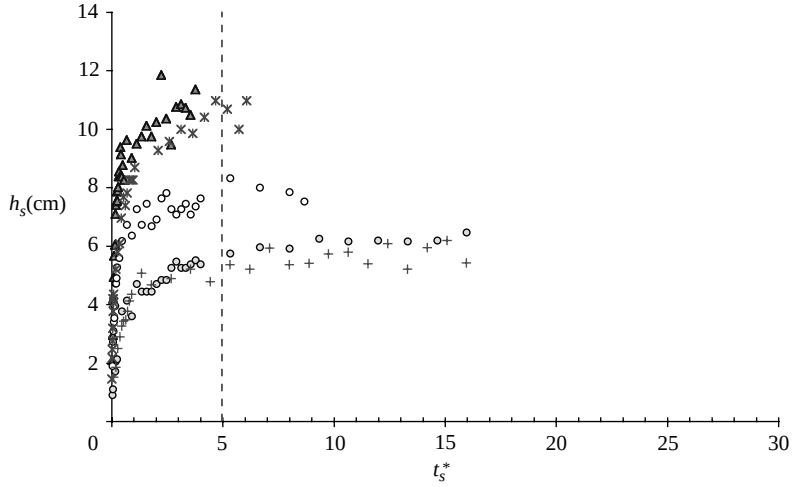

FIGURE 8. Maximum quasi-steady-state scour-hole depth, h_s versus time normalized by T_s, $t_s^* = t/T_s$. For definition of symbols see figure 7.

$h_s/b_0 = B_1((b_0/d_{50})^{-0.11} Fr_d^{1.1}) - B_2$ with $B_1 = 0.43$ and $B_2 = 0.2$. The value $B_1 = 0.43$ is close to $[C_6 \tan\varphi/\tau^*_{crit}]^{0.6/1.1} = 0.4$. A good correlation is therefore

$$\frac{h_s}{b_0} = \left[10^{-2}\frac{\tan\varphi}{\tau^*_{crit}}\right]^{0.55}\left(\frac{b_0}{d_{50}}\right)^{-0.11} Fr_d^{1.1} - 0.2. \tag{15}$$

The dependency of h_s on Fr_d or U_0 in (15) is close to the one proposed by Rajaratnam (1981) and Ali & Lim (1986) for h_a. The present scaling, inspired by the HHD model, also gives the dependency on the characteristics of the mobile bed material. Because of the narrow range of the experimental conditions, the exponent must be taken with some caution. Nevertheless, the weak dependency of h_s/b_0 on b_0/d_{50} given by $a \cong 0.6 \rightarrow \ell \cong 1.1$ is essential. Without it, the points for $b_0 = 2.5$ and 8 cm would not all collapse onto a straight line. Even more remarkable is the correct value of the pre-factor given by this scaling exponent.

The associated characteristic time scale for reaching quasi-steady-state conditions is more difficult to define experimentally. Adapting the HHD model (eqution (10)) for t_s, a time scale T_s can be defined in the form

$$T_s = \frac{(1-p)\,b_0^2}{8\left(\tau^{*3}_{crit}\,\Delta\,\rho g d_{50}^3/\rho\tan^3\varphi\right)^{1/2}}\, f_2(\Theta). \tag{16}$$

The function $f_2(\Theta) = (\Theta^{2/(1-\gamma)})^b$ expresses the dependency on U_0. A first and obvious choice is to take $b = 0$, which means that the time it takes to reach a quasi-steady state is independent of velocity, but depends strongly on b_0 (on b_0^2). In figure 8, h_s is plotted as a function of $t_s^* = t/T_s$ for $f(\Theta) =$ constant for three different gate openings b_0 and different velocities. In all cases, the quasi-steady state is reached for $t_s^* \approx 5$ and it is seen that the time, t_s indeed scales with b_0^2. No obvious velocity dependency emerges. If anything, the exponent b would need to be small, but negative.

With the scales H_s and T_s, the transport equation can still be written in non-dimensional form provided that

$$Q_s = 8\left(\tau^{*3}_{crit}\,\Delta\,\rho g d_{50}^3/\rho\tan^3\varphi\right)^{1/2}\left(\Theta^{1/1-\gamma}\right)^c \tag{17}$$

with $c = 0.6$.

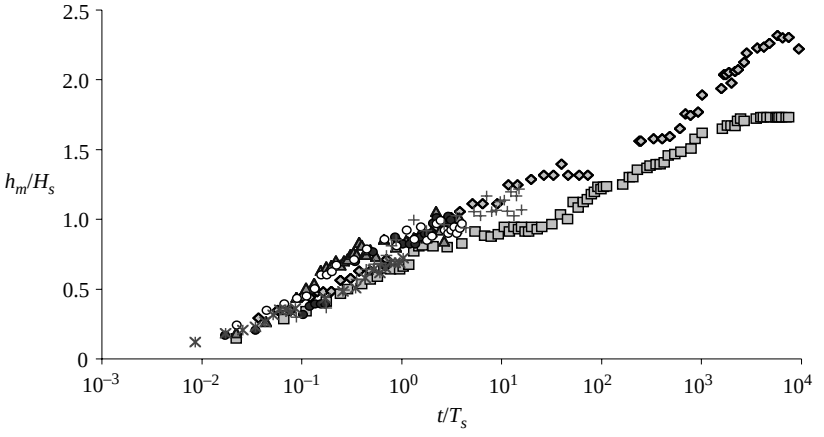

FIGURE 9. Maximum scour-hole depth normalized by H_s, h_m/H_s versus the logarithm of time normalized by T_s, t/T_s. For the correspondence of symbols see figure 5.

It is of interest to rescale the time evolution of the scour-hole depth by using the characteristic length and time scale H_s and T_s instead of H and T. This is done in figure 9; the collapse is as good as in figure 6. These new scaling laws do not mean that the HHD model is not correct. However, it could perhaps be reformulated in terms of the scales H_s, T_s and Q_s.

5. Conclusion and further discussion

The observed loose sediment streaks or longitudinal ridges (see figure 1) on the upstream-facing sediment slope of the scour hole are a signature of intense longitudinal vortices which lift up the sediment. The origin of these vortices is attributed to Görtler instability and it is shown that the flow conditions favour such an instability of the boundary region of the turbulent wall jet. The turbulent Görtler number (see table 1) is found to be well above the critical value, which implies that the vortices are intense and unsteady. The measured sediment streak spacing, representative of the wavelength, is shown to be consistent with the theoretical wavelength (see figure 4). To our knowledge, this is the first time that this sediment transport pattern, generated by longitudinal vortices, has been clearly identified and that their existence is linked to Görtler instability.

The contribution of these vortices to bed shear stress is likely to be of the same form as normal turbulent shear stress and is, therefore, additive (equation (4)). A numerical example is presented which shows that the Görtler vortices can increase the effective shear stress (shear stress effective in sediment transport) by an order of magnitude. Support for this increase of the shear stress by a constant factor is given by the HHD model which considers only a turbulent shear stress and contains adjustable constants. The time evolution of the scour-hole depth predicted by the HHD model is in good agreement with experiments. Indeed, when expressed in non-dimensional variables, all the data concerning the depth-time evolution collapse reasonably well onto a single curve (see figure 6) in the first scour regime, until a quasi-steady state (called steady state by HHD) is reached at $t = t_s$. This is the regime where the HHD model is valid.

Of practical interest are the asymptotic scour-hole depth, h_a and scour length, L_a. We consider here that $h_a = c_1 h_s$ and $L_a = c_2 L_s$, where $h_s = h_m(t_s)$ and $L_s = x_b(t_s)$ are

the quasi-steady-state scour-hole dimensions reached at $t = t_s$. The constants c_1 and c_2 vary between 1.5 and 2. It is shown that h_s scales on $h_s/b_0 = B_1((b_0/d_{50})^{-0.11} Fr_d^{1.1}) - B_2$ so that the characteristic length scale is $H_s = b_0 \Theta^{0.55}$ (equation (13)). The time t_s required to reach this quasi-steady state is practically independent of the jet velocity, but depends on b_0^2 according the characteristic time scale, T_s, given by equation (14). For practical applications, the scales H_s, T_s and Q_s are more useful scales than H, T and Q.

The second regime $t > t_s$ goes on for an extremely long time (see Tests B and C, figures 5 and 6) and no upper time limit can be given. Erosion is very slow and occurs partly by suspended load transport (see particles in suspension in figure 3*a*) and by an intermittent rearrangement of the downstream sediment slope. It is conjectured that without Görtler vortices, suspended load formation would not occur at $t > t_s$ and bed rearrangement would also be absent or considerably reduced. The Görtler vortices cause strong up-slope sediment transport and, in turn, strong avalanching which intermittently destabilizes the sediment hill.

The authors wish to thank M. S. Altinakar for his continued encouragement and A. Bottaro, for drawing their attention to the work of Tani (1962) and other papers on Görtler vortices. E. J. H. acknowledges a two-month visiting professorship at the EPFL. Financial support from the Swiss Federal Commission on Scholarships for Foreign Students to A. K. is gratefully acknowledged.

REFERENCES

Ali, K. H. M. & Lim, S. Y. 1986 Local scour caused by submerged wall jets. *Proc. Inst. Civil Engrs* **81**, 607–645.

Antonia, R. A. & Luxton, R. E. 1971 The response of a turbulent boundary layer to a step change in surface roughness. Part 1. Smooth to rough. *J. Fluid Mech.* **48**, 721–761.

Bottaro, A. & Luchini, P. 1999 Görtler vortices: are they amenable to local eugenvalue analysis. *Eur. J. Mech.* B/*Fluids* **18**, 47–65.

Chatterjee, S. S., Ghosh, S. N. & Chatterjee, M. 1994 Local scour due to submerged horizontal jet. *J. Hydraul. Engng ASCE* **120**, 973–992.

Clauser, F. H. 1956 The turbulent boundary layer. *Adv. Appl. Mech.* **4**, 1–51.

Eggenberger, W. & Mueller, R. 1944 Experimentelle und theoretische Untersuchungen ueber das Kolkproblem. *Mitteil. Versuchsanstalt f. Wasserbau*, no. 5, Zurich, CH.

Fujisawa, N. & Shirai, H. 1986 On the stability of turbulent wall jets along concave surfaces. *Bull. Japan Soc. Mech. Engng* **29**, no. 257, 3761–3766.

Floryan, J. M. 1989 Görtler instability of wall jets. *AIAA J.* **27**, 112–114.

Floryan, J. M. 1991 On the Görtler instability of boundary layers. *Prog. Aerospace Sci.* **28**, 235–271.

Görtler, H. 1941 Über eine dreidimensionale Instabilität laminarer Grenzschichten an konkaven Wänden. *Nachr. Wiss. Ges. Göttingen, Math. Phys. Klasse, Neue Folge* 2, no. 1 (1940), see also: *Z. Angew. Math. Mech.* **21**, 250–252 (1941).

Graf, W. H. 1971 *Hydraulics of Sediment Transport*. McGraw-Hill.

Graf, W. H. & Altinakar, M. S. 1998 *Fluvial Hydraulics*. J. Wiley.

Grass, A. J. 1971 Structural features of turbulent flow over smooth and rough boundaries. *J. Fluid Mech.* **50**, 233–255.

Hall, P. 1983 The linear development of Görtler vortices in growing boundary layers. *J. Fluid Mech.* **130**, 41–58.

Hall, P. 1990 Görtler vortices in growing boundary layers: the leading edge receptivity problem, linear growth and the nonlinear breakdown stage. *Mathematika* **37**, 151–189.

Hogg, A. J., Huppert, H. E. & Dade, W. B. 1997 Erosion by planar turbulent wall jets. *J. Fluid Mech.* **338**, 317–340 (referred to herein as HHD).

Karim, O. A. & Ali, K. H. M. 2000 Prediction of flow patterns in local scour holes caused by turbulent water jets. *J. Hydraul. Res.* **38**, 279–287.

Kobayashi, R. & Fujisawa, N. 1983. Turbulence measurements in wall jets along strongly concave surfaces. *Acta Mech.* **47**, 39–52.

Kobus, H., Leister, P. & Westrich, B. 1979 Flow field and scouring effects of steady and pulsating jets impinging on a movable bed. *J. Hydraul. Res.* **17**, 175–192.

Kurniawan, A., Altinakar, M. S. & Graf, W. H. 2001 Flow pattern of an eroding jet. *Proc. Cong. IAHR* 24, Beijing, pp. 537–544.

Kurniawan, A., Altinakar, M. S. & Graf, W. H. 2004 Scour depth and flow pattern of eroding plane jets. *Intl J. Sediment Res.* **19**, 15–27.

Luchini, P. & Bottaro, A. 1998 Görtler vortices: a backward-in-time approach to the receptivity problem. *J. Fluid Mech.* **363**, 1–23.

Matsson, O. J. E. 1995 Experiments on streamwise vortices in a curved wall jet flow. *Phys. Fluids* **7**, 2978–2988.

Meroney, R. N. & Bradshaw, P. 1974 Turbulent boundary-layer growth over a longitudinally curved surface. *AIAA J.* **13**, 1448–1453.

Rajaratnam, N. 1976 *Turbulent Jets.* Elsevier.

Rajaratnam, N. 1981 Erosion by plane turbulent jets. *J. Hydraul. Res.* **19**, 339–358.

Rajaratnam, N. & Berry, B. 1977 Erosion by circular turbulent wall jets. *J. Hydraul. Res.* **15**, 277–289.

Saric, W. S. 1994 Görtler vortices, *Annu. Rev. Fluid Mech.* **26**, 279–409.

Schlichting, H. 1968 *Boundary Layer Theory*. McGraw-Hill.

Tani, I. 1962 Production of longitudinal vortices in the boundary layer along a concave wall. *J. Geophys. Res.* **67**, 3075–3080.